



Full Length Article

Thermal stability of anti-reflective and protective a-C:H:SiO_x coating for infrared optics

A.S. Grenadyorov, A.A. Solovyev*, K.V. Oskomov, V.O. Oskirko, V.A. Semenov

The Institute of High Current Electronics SB RAS, 2/3, Akademicheskii Ave., 634055 Tomsk, Russia

ARTICLE INFO

Keywords:

Anti-reflective coating
SiO_x-doped amorphous hydrogenated carbon
Thermal stability
Mechanical properties

ABSTRACT

Poor mechanical and wear-resistant properties is the main weakness of infrared multi-layer anti-reflective optical coatings. The paper deals with anti-reflective and protective coatings based on SiO_x-doped amorphous hydrogenated carbon deposited on both sides of the polished single-crystalline silicon substrates. A method of plasma-enhanced chemical vapor deposition in a mixture of argon and polyphenylmethylsiloxane vapors is used for this coating. Anti-reflective properties of obtained coatings are studied by the Fourier-transform infrared spectroscopy. It is shown how the mechanical properties, chemical composition and wettability of the a-C:H:SiO_x coating depend on annealing in air. It is found that the average infrared transmission of the silicon substrates with double-sided film deposition is 87% in a 3–5 μm wavelength span, while the maximum infrared transmission is about 90%. At the same time, the films have excellent mechanical properties, heat resistance to 500 °C, and chemical resistance to a sea salt solution. The obtained anti-reflective coating has a great potential to be used as an anti-reflective and protective coating for infrared optical silicon products.

1. Introduction

Recently, in the development of infrared (IR) equipment based on silicon and germanium, much attention has been paid to the surface protection from physical impact and the improvement of transparency in the IR spectral region. A key role in this region plays the average wavelength ranging from 3 to 5 μm. The infrared atmospheric window in this range is suitable for various infrared technologies both in civilian and military applications [1]. Fluoride- and chalcogenide-containing multi-layer anti-reflective (AR) films are usually used to ensure high transparency of IR optical silicon products [2–5]. Weaknesses of such films include low mechanical and wear-resistant properties and, as a consequence, they must be re-deposited for optical reuse [6]. Due to the long wavelength infrared region, the coating thickness is usually equal to hundreds of nanometers. Therefore, a multilayer oxide AR film may crack during its deposition due to no adhesion or internal stresses [7].

In this regard, carbon-based films (a-C, a-C:H, etc.) are of great interest as they have excellent mechanical and tribological properties and capable of providing high transmittance to the infrared optical silicon elements. Pan, et al. [3] used diamond-like carbon (DLC) coatings as a mechanical and environmental protection of the AR coating consisting of fluoride and chalcogenide layers. They used a zinc selenide substrate with about 73% average transmission in the IR spectral region. It was

shown that after the deposition of the protective DLC coating, the mechanical and environmental durability of the AR coating was significantly improved. At the same time, the average transmission of the DLC AR coating was 93.1% in the 2–16 μm range, which was consistent with the simulation results obtained in [3].

Zhang, et al. [8] showed that the infrared transmission of Ge substrate with the DLC film deposited on both sides by capacitively coupled plasma driven by 13.56 MHz radiofrequency in 2.5–15 μm range averaged out to 85%, with a 97% maximum. In [4] Ankit, et al. deposited the DLC film onto both sides of Ge substrate, which provided its transmission peak of 93% at a 5 μm wavelength, 32.7 GPa average hardness and 246.1 GPa modulus of elasticity. In [5], Reddy, et al. deposited DLC onto both sides of a single-crystal silicon substrate by the radio frequency plasma-enhanced chemical vapor deposition (PECVD) method, which increased the maximum IR transmission from 55 to 89% at a 4.5 μm wavelength.

However, DLC films also have weaknesses. Miller, et al. [9] mentioned that internal stresses in diamond and diamond-like films, accumulated during their formation, caused insufficient adhesion to Ge substrates. Heeg, et al. [10] reported that the thickness of the DLC film deposited onto Ge substrate having 160 °C temperature should be not over 600 nm. Otherwise, internal stresses significantly increased and lowered the adhesion. Varade, et al. [11] studied the temperature effect

* Corresponding author.

E-mail address: andrewsol@mail.ru (A.A. Solovyev).<https://doi.org/10.1016/j.apsusc.2020.145433>

Received 24 October 2019; Received in revised form 10 January 2020; Accepted 15 January 2020

Available online 18 January 2020

0169-4332/ © 2020 Elsevier B.V. All rights reserved.

on the IR transmission from polished Ge substrate during the radio frequency PECVD of the DLC film. It was shown that the DLC film obtained at room temperature possessed higher IR transmission than the film deposited at 150 °C. The DLC film deposited at room temperature onto both sides of Ge substrate enhanced the transmission peak up to 90% in 3–6 μm IR spectral region, while the film deposited at 150 °C enhanced it only up to 65%. It was also shown that the increased content of sp³ hybridized carbon atoms in the DLC film caused the coating adhesion deterioration.

One of the types of carbon films is SiO_x-doped amorphous hydrogenated carbon (a-C:H:SiO_x) film, also known as a diamond-like nanocomposite or SiO_x-doped DLC film. This type is characterized by relatively high hardness (10–20 GPa), low friction coefficient (0.02–0.2) and wear rate (10⁻⁵–10⁻⁸ mm³ N⁻¹ m⁻¹), high transmission (~80–85%) in the visible spectral region [12–15]. In addition, a-C:H:SiO_x films are characterized by low internal stresses (less than 1 GPa) due to the presence of Si–C bonds (1.89 Å) which are longer than C–C bonds (1.54 Å) [16]. This provides excellent adhesion to the majority of substrates and the formation of films with a thickness ranging from several to tens of micrometers.

According to [15,17], the optical properties of a-C:H:SiO_x films in the visible wavelength range allowed them to be used as AR coatings for silicon-based solar cells. However, to the authors' best knowledge, the anti-reflective properties of a-C:H:SiO_x films in the IR spectral region have never been investigated. The film structure and properties depend on the deposition parameters and post-deposition treatment. The effect of post-deposition annealing on structural and optical properties of a-C:H:SiO_x films is described in [15,18], whereas this effect on anti-reflective properties of a-C:H:SiO_x films has not been reported so far.

This work involves the PECVD method for a-C:H:SiO_x films onto silicon substrates and suggests a technique that improves the adhesive and protective properties of the proposed heat-resisting AR coatings.

2. Experimental

Double-sided surface-polished substrates 20 × 20 mm² in size, made of monocrystalline silicon with (1 0 0) crystallographic orientation, with 720 Ohm·cm resistivity and 350 μm thickness were used for the film deposition. Before loading into the vacuum chamber, the substrates were processed in an ultrasonic bath filled alternately with isopropyl alcohol, acetone, and distilled water. In each of the liquids, the substrates were cleaned for 3 min.

The a-C:H:SiO_x films were deposited by the plasma-enhanced chemical vapor deposition (PECVD) method based on non-self-sustained arc discharge with the hot cathode as described in detail in [19]. Polyphenylmethylsiloxane (PPMS) was used as a liquid precursor for the film formation. PPMS was fed into the precursor ejection head (de Laval nozzle) near the tungsten hot cathode. The de Laval nozzle was heated by the IR radiation and electrons emitting from the hot cathode resulting in PPMS evaporation. The residual pressure in the vacuum chamber was 10⁻² Pa. Prior to the film deposition the substrate surface underwent plasma cleaning in argon gas. The process parameters of plasma cleaning included 0.3 Pa pressure, 1000 V amplitude of negative pulses of the bias voltage, 100 kHz pulse repetition rate, a 60% duty cycle, 50 A filament cathode current, 11 A discharge current, and 100 V discharge voltage. The magnetic field induction nearby the substrate was 3 G. After plasma cleaning, the a-C:H:SiO_x films were subjected to PECVD in a mixture of argon and PPMS vapors. The PECVD process parameters included 0.1 Pa pressure, 5.5–6 A discharge current, 140 V voltage, 500 V amplitude of negative pulses of the bias voltage, and 70 ± 10 nm/min deposition rate.

The film transmittance in the IR spectral region was studied on a Nicolet 5700 FTIR Spectrometer (Thermo Fisher Scientific, USA). Fourier-transform infrared (FTIR) spectra were analyzed within a 400–4000 cm⁻¹ spectral range, with a resolution of 4 cm⁻¹. The samples were annealed in air, in a high-temperature furnace

(Nabertherm, Germany) at heating and cooling rates of 50 degrees per hour, for 2 h. Mechanical properties of the obtained films were measured by the instrumented indentation technique using the Oliver–Pharr relation. The indentation load of the Nanotest 600 nano-hardness tester (Micro Materials Ltd., GB) was 20 mN. The surface morphology of the obtained films was studied on a Solver P47 Atomic Force Microscope (AFM) (Russia) and the Quanta 200 3D (Netherlands), a dual-beam scanning electron microscope (SEM). Raman spectroscopy is used to explore the film structure. Using the Centaur U HR system (532 nm laser) Raman spectra were measured in 1000–2000 cm⁻¹ range with the spectral resolution of 1.5 cm⁻¹. For the analysis of the elemental composition we used the X-ray photoelectron spectrometer (XPS) (SPECS Surface Nano Analysis GmbH, Germany) equipped with a SPECS FOCUS 500 ellipsoidal monochromator, a SPECS PHOIBOS 150 hemispherical energy analyzer with MCD-9 detector for photoelectron spectroscopy measurements, with XR-50 and XR-50R X-ray sources with Al/Mg and Al/Ag dual anodes and catalytic cell. The X-ray photoelectron spectra were measured with monochromatized Al K_α radiation ($h\nu = 1486.74$ eV) in the energy range of 0–1100 eV with 0.5 eV spectral resolution. The contact angle measurement with EasyDrop system (Kruss GmbH, Germany) utilized distilled water as a laboratory fluid.

3. Results

3.1. Transmission of a-C:H:SiO_x films on Si substrates

It is known that the relationship between the thickness of AR coatings and the wavelength is as follows:

$$\lambda = 4dn$$

where d is the thickness of the AR layer; λ is the wavelength which must correspond to the minimum reflectivity; n is the refractive index of the AR layer.

The a-C:H:SiO_x film refractive index of 1.8 was obtained by the reflecting ellipsometry method at a wavelength of 1050 nm. This value was used to estimate the film thickness which provided anti-reflection in the IR spectral region between 3 and 5 and 4–8 μm. Accordingly, the thickness of the AR layer should be ~550 and 830 nm to ensure a minimum reflection at 4 and 6 μm wavelengths.

Firstly, three Si substrates were used to determine the infrared transmission. The first and the second substrates were coated with a-C:H:SiO_x films 500 ± 50 and 750 ± 50 nm thick, respectively, the third substrate being uncoated. Secondly, both sides of another two Si substrates were coated by the similar film layers, and the third substrate also being uncoated. According to the results of FTIR measurements presented in Fig. 1, the transmission spectra were improved. FTIR measurements were carried out in the IR spectral region within the wavelength range of 2.5–10 μm.

As can be seen from Fig. 1, the increased film thickness leads to a shift in the anti-reflective region towards larger wavelengths. Fig. 1a, shows that the single-sided film deposition improves the IR transmission of bare Si from 50 to 67% at a 4.1 μm wavelength (curve 1) and to 66% at a 6 μm wavelength (curve 2). Similarly, according to Fig. 1b, the double-sided film deposition improves the IR transmission further to 90% with the peak transmission at a 3.8 μm wavelength (curve 1) and to 93% with the peak transmission at a 5.9 μm wavelength (curve 2). For the Si substrates with the double-sided deposition of 500- and 750-nm-thick films, the integral transmission is 87 and 81%, respectively for the wavelength ranges of 3–5 and 4–8 μm. The measured transmission is not lower than the values obtained for un-doped DLC films (a-C:H) in [4,5].

The substrates with the double-sided film deposition were annealed in air at 250, 500 and 600 °C for two hours. Fig. 2 presents FTIR spectra of Si substrates with the deposited films 500 and 750 nm thick, annealed at different temperatures. Table 1 presents the maximum and

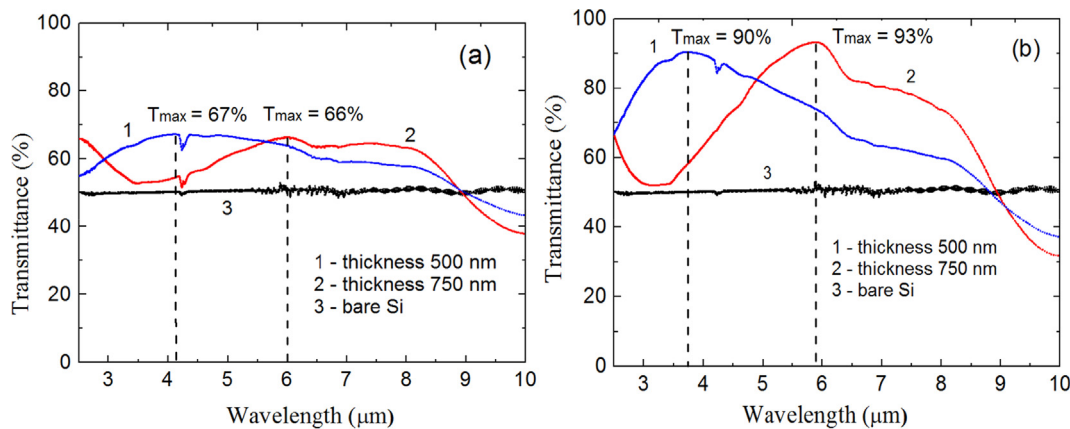


Fig. 1. FTIR spectra in the IR region in the 2.5–10 μm wavelength range: a – single-sided, b – double-sided deposition of a-C:H:SiO_x films.

integral values of the transmission of the samples, determined from the FTIR spectra. After annealing, the spectra shift to the region of shorter or longer wavelengths, but, in limited wavelength range (3–5 or 4–8 μm), the transmission of the samples increases. In particular, for the 500 nm thick film, the peak transmittance increased from 90 to 94% after heat treatment at 500 °C. However, as the annealing temperature is increased to 600 °C, both peak and integral transmission values begin to decrease slightly.

Changes in the FTIR spectra, as will be shown below, are associated with a change in the chemical composition and structure of the films. In addition, they can be caused by a decrease in film thickness as a result of carbon and hydrogen oxidation and degassing during the high-temperature annealing process [20]. After annealing at 500 °C, a pronounced Si–O–Si absorption peak at a wavelength of 9.2 μm (1090 cm⁻¹) [21] appears in the spectra. At a temperature of 600 °C, its intensity increases. This indicates an increase in the content of silicon and oxygen in the film.

3.2. Mechanical properties of a-C:H:SiO_x films on Si substrates

The important function of AR films is the surface protection of optical products. Such films must therefore have high mechanical and tribological properties which prevent optical products from the surface abrasion and scratching. The main mechanical properties include hardness (*H*), elastic modulus (*E*), plasticity index (*H/E*), resistance to plastic deformation (*H³/E²*) and elastic recovery *W_e*. Table 2 summarizes the mechanical properties of the films subjected to thermal annealing in air at temperatures from 100 to 600 °C to estimate their thermal stability. It should be noted that, initially, the film is

Table 1

The transmittance in the IR region of Si substrates with double-sided deposition of a-C:H:SiO_x films after annealing.

Sample	Transmittance of 500 nm thick film (peak/integral value in the 3–5 μm region), %	Transmittance of 750 nm thick film (peak/integral value in the 4–8 μm region), %
As-deposited	90/86.8	93/81.4
AT = 250 °C	92/86.3	93.5/81.8
AT = 500 °C	94/89.4	92.9/82.3
AT = 600 °C	93.5/87.7	93.1/82

Table 2

Mechanical properties of a-C:H:SiO_x films before and after annealing.

Sample	<i>H</i> (GPa)	<i>E</i> (GPa)	<i>H/E</i>	<i>H³/E²</i> (MPa)	<i>W_e</i> (%)
As-deposited	20.1	152	0.132	352	78
AT = 100 °C	18.86	149.6	0.126	300	80
AT = 250 °C	19.01	140.5	0.135	348	79
AT = 300 °C	18.63	140.8	0.132	326	80
AT = 400 °C	18.51	146	0.126	297	78
AT = 500 °C	19.09	154.9	0.123	290	79
AT = 550 °C	12.04	138	0.087	92	70
AT = 600 °C	10.64	134.1	0.079	67	67

characterized by 20.1 GPa hardness, 0.13 plasticity index, 352 MPa plastic resistance, and a high degree of elastic recovery (78%). Annealing at temperatures up to 500 °C slightly affects the mechanical properties of the film. The hardness of the films ranges from 18.5 to 19 GPa. 500 °C annealing insignificantly reduces the mechanical

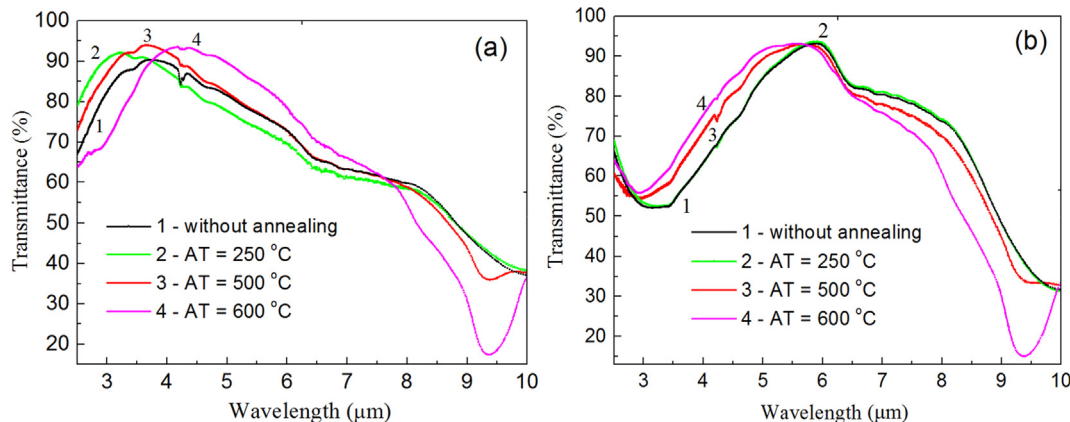


Fig. 2. FTIR spectra of Si substrates with double-sided deposition of a-C:H:SiO_x films for different annealing temperatures (AT): a – film thickness of 500 nm; b – film thickness of 750 nm.

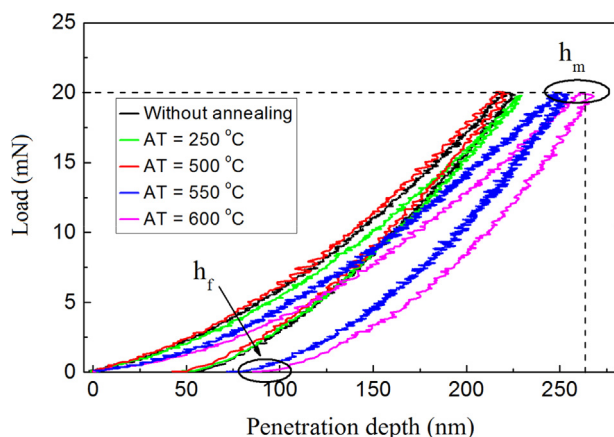


Fig. 3. Indentation load/unload curves of a-C:H:SiO_x films after thermal annealing in air (h_m – maximum depth, h_f – final depth).

properties of the films, in particular, 5% and 18% decrease is observed in H and H^3/E^2 values, respectively. The elevation of annealing up to 550 °C leads to a drastic decrease in all the mechanical properties of the film. The hardness reduces to 12.04 GPa and the resistance to plastic deformation to 92 MPa. After annealing at 600 °C, all mechanical characteristics continue to decrease.

The degree of the elastic recovery is the important parameter of solid films which shows how much the film recovers after deformation. Using the indentation load/unload curves, this parameter can be calculated as

$$W_e = \frac{h_m - h_f}{h_m} \cdot 100\%$$

where h_m is the maximum indentation depth (nm), h_f is the residual indentation depth after unloading (nm).

Fig. 3 shows the indentation load/unload curves for a-C:H:SiO_x-coated Si samples after annealing at different temperatures. The increase in the annealing temperature up to 500 °C does not significantly change the indentation load/unload curves. This suggests that the degree of the elastic recovery does not change and amounts to 78–79%. The annealing temperature elevated up to 600 °C results in the increase in the indentation depth, thereby producing the elastic recovery decrease down to 67%.

The critical temperature at which the properties of the film begin to change is 550 °C for the obtained a-C:H:SiO_x films. This value is much larger than that of amorphous carbon films. According to Yang, et al. [22] annealing of amorphous carbon at temperatures above 200 °C leads to a modification of its structure and properties. A high concentration of (–Si–O–) bonds in carbon coating allows achieving the higher thermal stability of the material [18,22]. As reported, when the thermal annealing exceeds 300 °C, the DLC-SiO_x coating properties modify. The structure of DLC-SiO_x coatings is affected neither by 400 °C nor 600 °C vacuum-assisted thermal annealing, but it is affected by 400 °C thermal annealing in the air [18].

The possible reason for influencing the thermal treatment is the film graphitization, i.e. transformation of sp³ into sp² hybridized carbon. Another reason is the interaction between oxygen from air and carbon atoms in the coating resulting in the formation of carbon dioxide and its degassing. Both of these reasons are confirmed by further experiments.

3.3. Surface morphology of a-C:H:SiO_x films

Fig. 4 contains 3D atomic force microscopy images of the as-deposited coating surface and after 250, 500 and 600 °C annealing in air. Coatings have a smooth surface, without a pronounced granular structure. This indicates to the amorphous coating structure. It is worth noting that with the annealing temperature elevated up to 600 °C, the

root mean square (RMS) roughness increases from 0.36 to 1.2 nm (see the Z-axis scale). On the surface of the film, there are small convexities with a diameter of about 200 nm and a height of only a few nm (note that the Z-axis scale does not coincide with the scale of the X, Y axes). After annealing at a temperature of 600 °C, the number of these convexities increases sharply.

In Fig. 5, SEM images of the a-C:H:SiO_x film surface are obtained before and after annealing. One can see that very smooth and uniform surface becomes rougher after annealing and contains nanoprotusions. The highest concentration of these nanoprotusions is observed on the film surface after 600 °C annealing, which is consistent with the AFM results.

3.4. Raman spectroscopy

In order to understand the temperature effect on the coating structure, its Raman spectra were investigated in the 1000–1800 cm^{−1} wavenumber range. The Raman spectra measured before and after annealing in air, were deconvoluted into Gaussian peaks by the curve fitting. Earlier analysis of Raman spectra of a-C:H:SiO_x films were performed by decomposition into two peaks, namely the D-peak and the G-peak [23]. However, at high annealing temperatures this method does not describe well the experimental data [24,25]. At least four peaks have to be used for amorphous hydrogenated carbon films in order to obtain more accurate data fitting [26]. In the case of silicon-doped DLC films five peaks had to be used to obtain a good fit [27]. In our case, the four-peak fitting of the Raman spectra turned out to be optimal (Fig. 6). The spectra contain two D peaks (D₁ and D₂) and two G peaks (G₁ and G₂). According to the literature [26] the high-frequency peak at 1585 cm^{−1} corresponds to the crystalline graphite peak and is called accordingly the G₁ band. The second peak at 1490 cm^{−1} corresponds to amorphous sp²-carbon and is called the G₂ band. The third peak at 1350 cm^{−1} corresponds to the polycrystalline graphite (disorder peak of graphite) and is assigned as the D₁ band. The fourth peak at 1130 cm^{−1} corresponds to the amorphous sp³-carbon (disordered sp³) and is named the D₂ band.

Despite the fact that the spectrum of as-deposited film is well approximated by two peaks, for consistency, we used four peaks for all spectra. The G₁ peak increases as the annealing temperature increases, while its full width at half maximum (FWHM) decreases from ~144 cm^{−1} to ~120 cm^{−1} for the films annealed at 200 and 700 °C, respectively. G₂ peak decreases with the growth of the annealing temperature. The increase and sharpening of the G₁ peak with a simultaneous decrease in intensity of the G₂ peak can be explained by increasing the in-plane ordering of sp²-carbon atoms. The same effect was observed for fluorinated a-C:H films with the growth of the annealing temperature [26]. The increasing of D₁ peak is another consequence of an increase in the annealing temperature, connected with the growth of very small graphitic regions.

3.5. X-ray photoelectron spectroscopy

Fig. 7 shows the XPS spectra of a-C:H:SiO_x coatings annealed in air at different temperatures. It is interesting to note, that with increasing annealing temperature, the intensities of the main peaks change. In particular, the increase in O1s (534 eV), Si2s (154 eV) and Si2p (102 eV) core-level peaks and the decrease in C1s (284 eV) core-level peak results from chemical changes in the film associated with the destruction of previous and the formation of new chemical bonds.

Consider Fig. 8, which plots the XPS curves for the Si2 peak of a-C:H:SiO_x films and its fitting using Lorentzian and Gaussian functions. With increasing annealing temperature the Si2p peak shifts to higher binding energies and widens. The Si2p peak of as-deposited film can be deconvoluted into two peaks. The first Si2 peak at lower binding energy of 100.5 eV belongs to Si–C bonds. The second Si2 peak observed at 102.1 eV, is consistent with the presence of (–Si(R₁)(R₂)–O–)_n

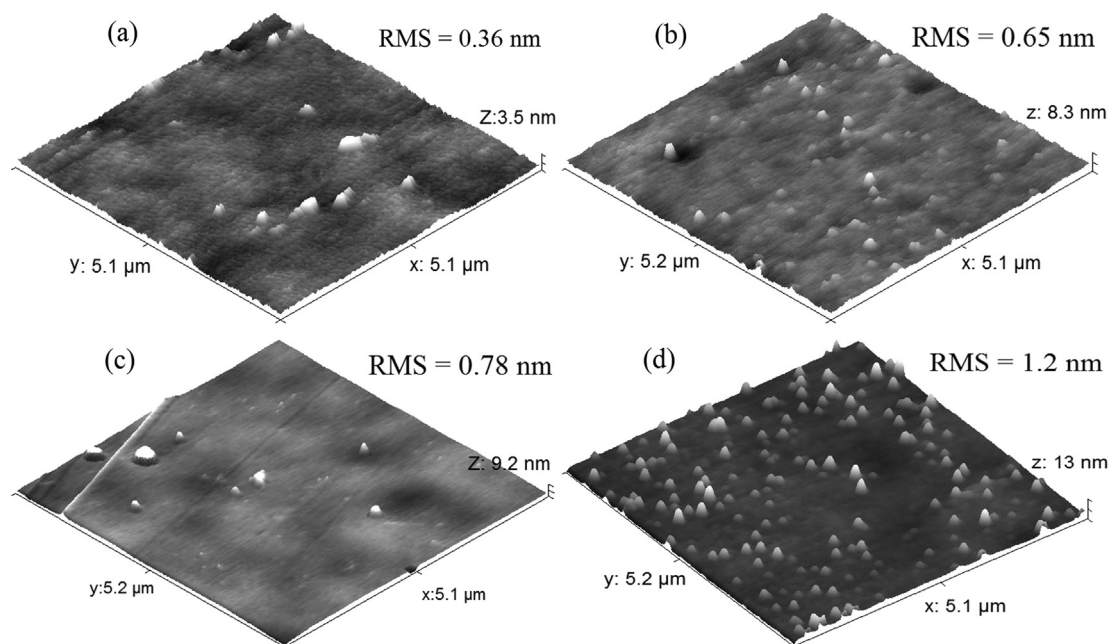


Fig. 4. 3D AFM images of $5 \times 5 \mu\text{m}^2$ size of a-C:H:SiO_x film surface after annealing at different temperatures: *a* – as-deposited, *b* – 250 °C, *c* – 500 °C, *d* – 600 °C.

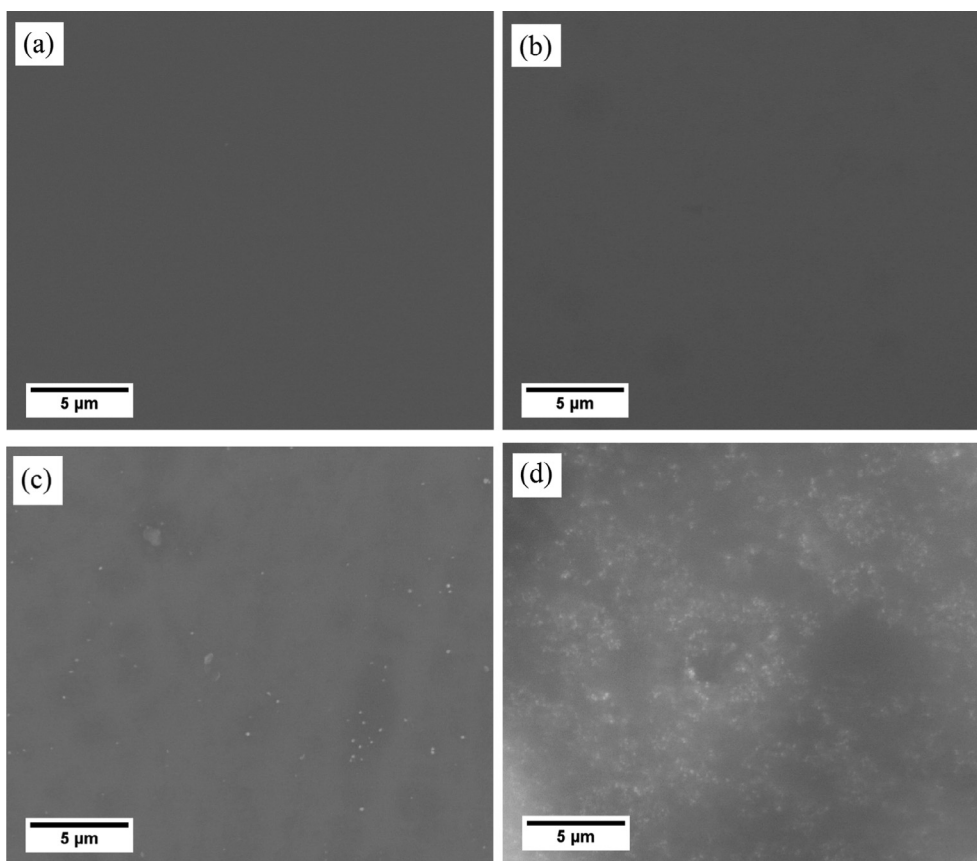


Fig. 5. SEM images of a-C:H:SiO_x film surface after annealing at different temperatures: *a* – as-deposited, *b* – 250 °C, *c* – 500 °C, *d* – 600 °C.

siloxane polymers, where R_1 and R_2 are aliphatic and/or aromatic organic structures [23]. After the film annealing at 250 °C, the Si2p peak is deconvoluted into one peak with a 102.6 eV binding energy. Owing to the substitution of carbon atoms by oxygen atoms during annealing, the Si2p peak shifts to the higher binding energy range, and the peak matching Si–C bond disappears. At an energy of 105.2 eV, the new Si2p

peak appears in samples subjected to 500 and 600 °C annealing. This peak indicates to the SiO₂ bond formation [28].

Fig. 9 shows the C1s peak of a-C:H:SiO_x films annealed in air at different temperatures. The C1s peak is deconvoluted into three different peaks with the binding energies of 284.3 ± 0.2 , 286.1 ± 0.2 and 288.2 ± 0.3 eV. The peak centered at 284.3 eV belongs to the C–C

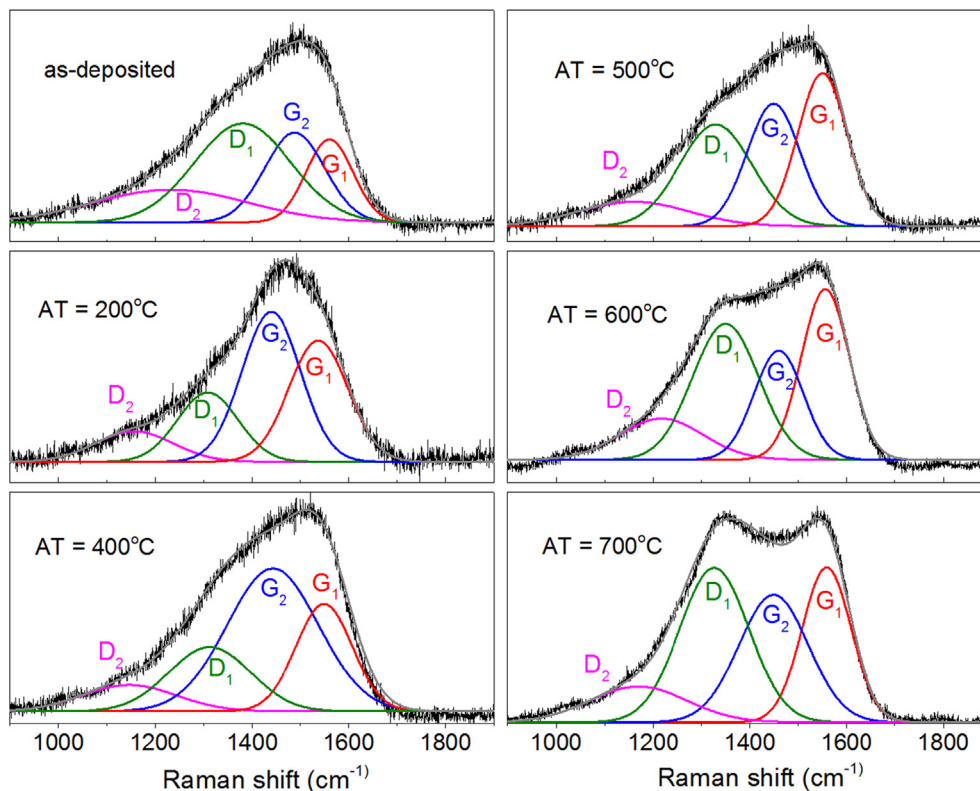


Fig. 6. Raman spectra of a-C:H:SiO_x films after annealing at different temperatures. Black lines represent the measured data; the color lines show the decomposition into four Gaussian peaks and gray lines the sum of these.

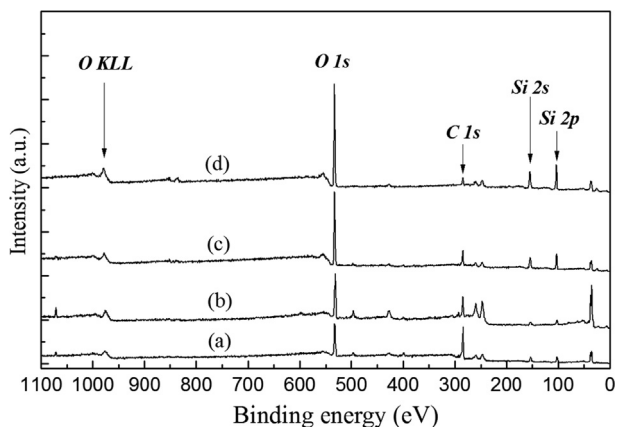


Fig. 7. XPS spectra of a-C:H:SiO_x films obtained after different annealing temperatures: a – as-deposited, b – 250 °C, c – 500 °C, d – 600 °C.

bonds with sp^2 and sp^3 hybridization [29]. The other two peaks of lower intensity match carbon-oxygen bonds at binding energies of 286.1 and 288.2 eV for C–O and CCO, respectively [30].

Fig. 10 shows the O1s peaks of a-C:H:SiO_x films annealed in air at different temperatures. Notably, the peak width decreases with increasing annealing temperature. The O1s peak is deconvoluted into two different peaks with binding energies of 530 ± 0.2 and 532 ± 0.4 eV. The peak at 530 eV indicates to C=O bonds and the peak at ~532 eV indicates to C–O bonds [28].

Table 3 presents the elemental composition of a-C:H:SiO_x films depending on the annealing temperature. With the temperature elevation, the carbon content in the film gradually lowers, while the content of silicon and oxygen increases. Accordingly, the C/Si ratio decreases from 4.2 to 0.25. The traces of nitrogen, sodium, and tungsten observed in the film can be explained by the presence of residual air during the

deposition process, surface contamination during the sample transportation, and evaporation of the tungsten filament, respectively.

3.6. Contact angle measurements

Fig. 11 shows images of a sessile drop on the surface of samples with a-C:H:SiO_x film after annealing in air. It is seen that an increase in the annealing temperature to 500 °C leads to an increase in the contact angle with water from 43 to 73°.

The increase in the contact angle is most likely associated with the increased Si content in the coating due to the elevated annealing temperature (see Table 3). Ogwu, et al. [31] find that Si doping of a-C:H films enhances their hydrophobicity due to the formation of Si–C and Si–H hydrophobic bonds. These bonds are responsible for the contact angle increase on the a-C:H:Si film surface due to larger Si amount. These chemical bonds minimize the surface-water interaction because of their low polarity, thereby lowering the polar component of the surface energy relative to the total surface energy.

3.7. Chemical resistance to sea salt solution

The operation of optical elements with AR coatings in aggressive environmental conditions results in the destruction and degradation of the coating surface. For example, in humid sea air, salt precipitates on the optical product surface and can destroy the coating. Therefore, the as-deposited coating was tested in compliance with the US military standard MIL-C-48497A “Coating, Single or Multilayer, Interference: Durability Requirements for”. In accordance with paragraph 4.5.5.2 of this standard, the coating should not be destroyed after the immersion in a sea salt solution (170 g of salt per 4.5 L of water at room temperature) for 24 h. Upon extraction from the solution, the samples are washed with distilled water and dried. The surface is then inspected for damage (peeling, cracks, etc.) using an optical microscope (Fig. 12).

Despite the fact that we immersed the coated samples in a sea salt

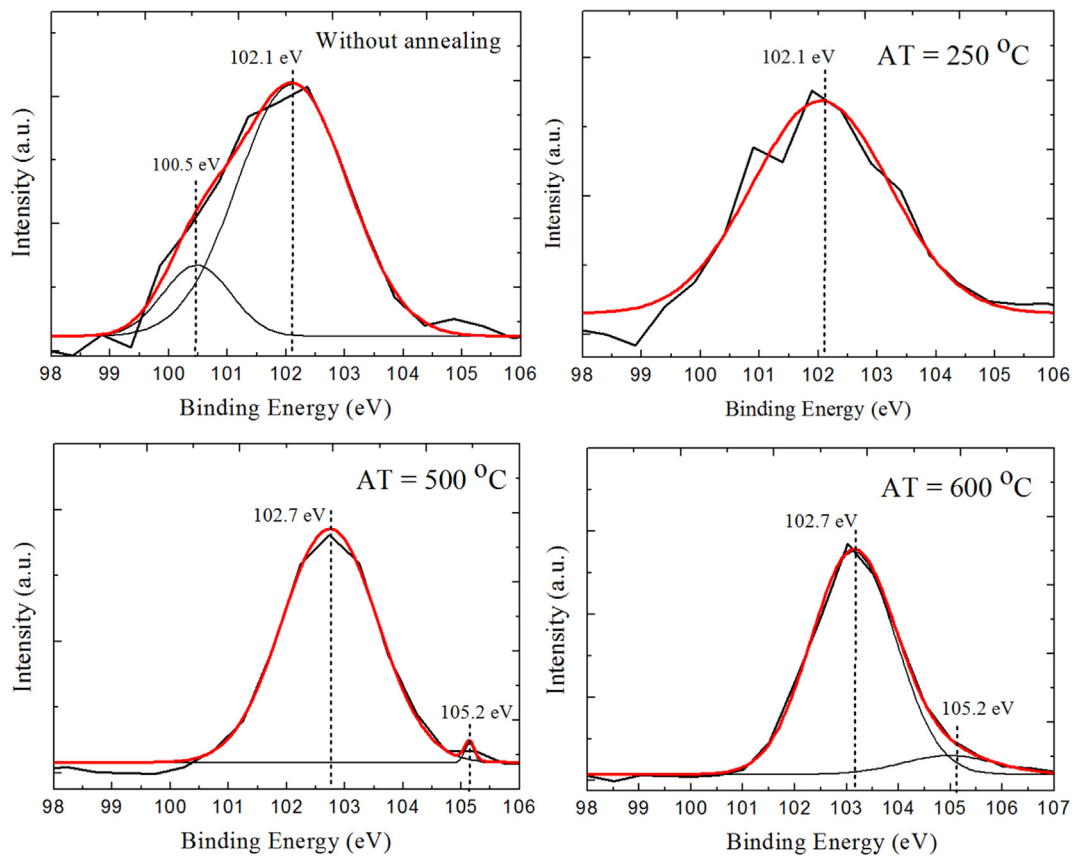


Fig. 8. Si2p XPS core-level peaks of a-C:H:SiO_x films annealed at different temperatures in air and the fitting results.

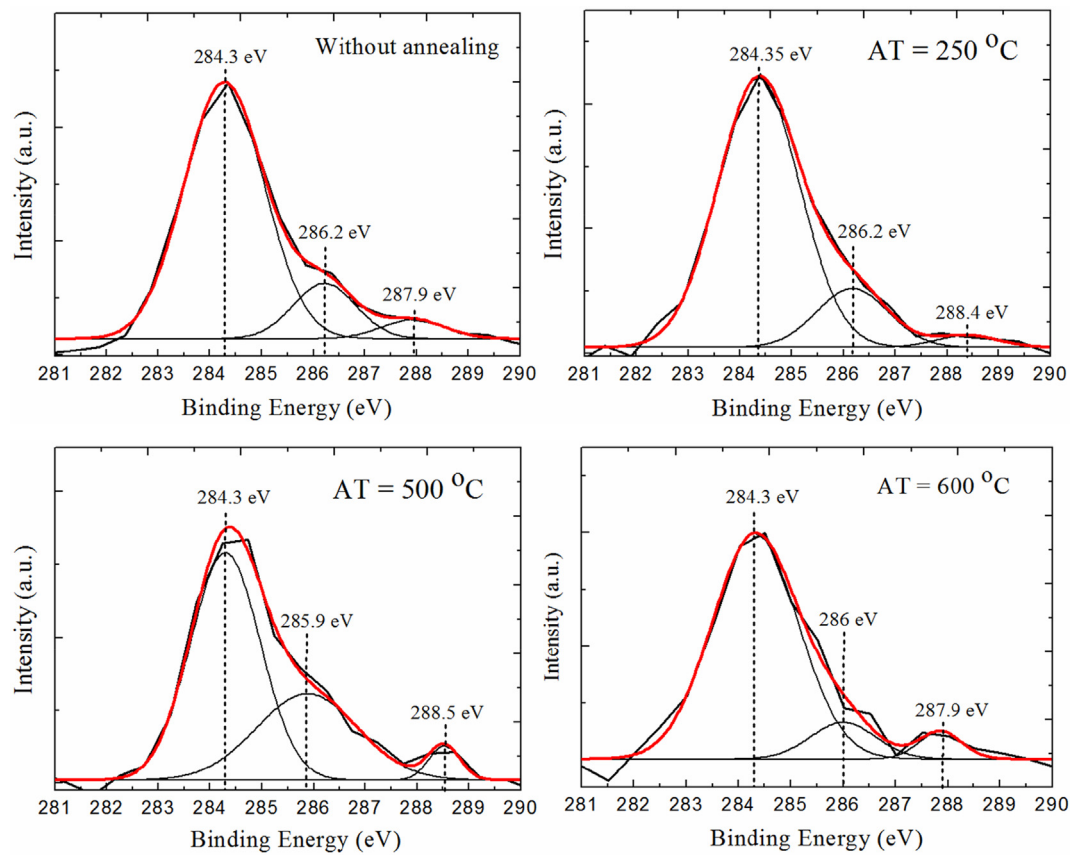


Fig. 9. C1s XPS peaks of a-C:H:SiO_x films annealed in air at different temperatures and the fitting results.

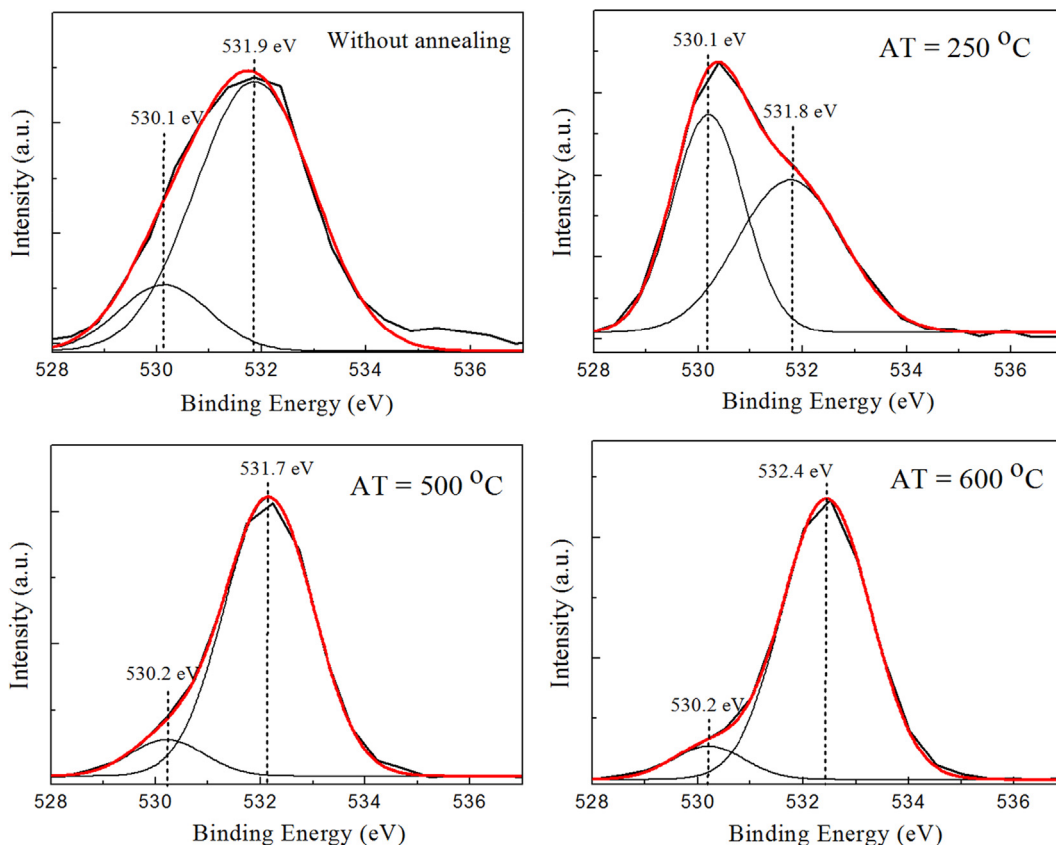


Fig. 10. O1s XPS peak of a-C:H:SiO_x films annealed in air at different temperatures and the fitting results.

Table 3
Elemental composition of a-C:H:SiO_x films depending on the annealing temperature.

Annealing temperature, °C	Chemical composition, at. %						C/Si
	C	Si	O	N	Na	W	
0	55	13	24	4	1	3	4.2
250	40	14	29	5	2	10	2.9
500	28	28	40	2	-	2	1
600	11	40	47	-	-	2	0.28

solution for 5 days (120 h), after the sample extraction, the AR coating was not destroyed. The coating retained its uniform and smooth structure.

4. Conclusion

It was shown that a-C:H:SiO_x coatings can be appropriately used as protective AR coatings for optical silicon elements in the mid-infrared (3–5 μm) wavelength range. The thermal stability, anti-reflective and mechanical properties of PECVD-deposited coatings on Si (1 0 0) were investigated. It was shown that in the case of the double-sided deposition of 500-nm-thick coatings on the Si substrate, the integral transmission in the 3–5 μm wavelengths range increased from 50 to 87%. Moreover, the coating displayed good mechanical properties, such as 18 GPa hardness, 0.13 plasticity index, 325 MPa plastic resistance, and 78% elastic recovery. In addition to good optical and mechanical properties, the coating possessed excellent thermal stability in air (up to 500 °C) and chemical resistance to the sea salt solution. The coating hardness was constant until annealing up to 500 °C, but significantly decreased at 600 °C. At 600 °C annealing temperature, a drastic degradation of all the mechanical properties was observed. The intensity ratio in the Raman spectra of the annealed a-C:H:SiO_x coatings started to increase from 500 °C, which indicated to the enlarged number of sp²-hybridized carbon atoms in the film or its graphitization. It was found that the chemical composition of the coating was changed with the temperature elevation. Thus, the carbon content gradually lowered, whereas the content of silicon and oxygen increased.

In conclusion, it is evident that thermal stability of a-C:H:SiO_x coatings is sufficient for the high-temperature protection and anti-reflective applications in air.

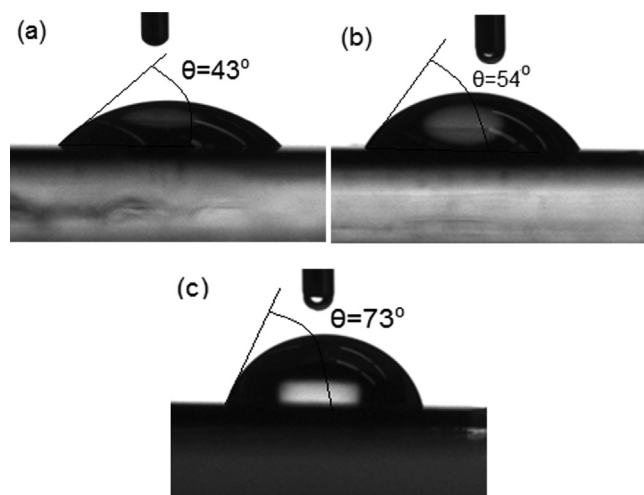


Fig. 11. Optical images of sessile drop measurements using a contact angle meter for the a-C:H:SiO_x film surface annealed at different temperatures in the air: a – as-deposited, b – 250 °C, c – 500 °C.

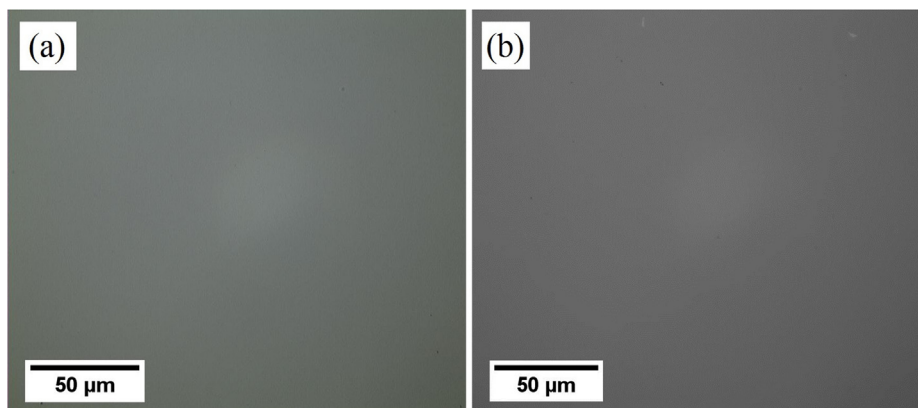


Fig. 12. Images of the surface of a-C:H:SiO_x coating before (a) and after (b) immersion in sea salt solution (optical microscopy).

CRedit authorship contribution statement

A.S. Grenadyorov: Conceptualization, Writing - original draft. **A.A. Solovyev:** Supervision, Methodology, Writing - review & editing. **K.V. Oskomov:** Visualization, Investigation. **V.O. Oskirko:** Investigation, Validation. **V.A. Semenov:** Investigation, Visualization.

Declaration of Competing Interest

The authors declare that they have no known competing financial interests or personal relationships that could have appeared to influence the work reported in this paper.

Acknowledgements

A study of the thermal stability and optical properties of a-C:H:SiO_x films was carried out within the government contract of the Institute of High Current Electronics SB RAS (N 0366-2019-0010). The investigation of the chemical composition, mechanical properties, and wettability of the films was financially supported by Grant N 19-19-00186 from the Russian Science Foundation.

The authors like to express their gratitude towards the management of the Tomsk Regional Core Facility Center of the TSC SB RAS for their support with the Nanotest 600 nanohardness tester, the Solver P47 atomic force microscope and the Nicolet 5700 FTIR spectrometer. We are grateful to the National Center of Catalyst Research for kindly providing the X-ray photoelectron spectrometer. We also thank N. N. Ryabova, the leading engineer of the Institute of Petroleum Chemistry SB RAS, for her help on achieving FTIR results and valuable discussions and V.V. Kachev and A.V. Selivanova for their kind technical assistance.

References

- [1] D.M. Gates, W.J. Harrop, Infrared transmission of the atmosphere to solar radiation, *Appl. Opt.* 2 (1963) 887–898.
- [2] F. Maudeta, B. Lacroix, A.J. Santos, F. Paumier, M. Parailous, C. Dupeyrat, R. García, F.M. Morales, T. Girardeau, Towards perfect MWIR transparency using oblique angle deposition, *Appl. Surf. Sci.* 470 (2019) 943–950.
- [3] Y. Pan, L. Hang, Z. Wu, Y. Yin, Design and fabrication of ultra-broadband infrared anti-reflection hard coatings on ZnSe in the range from 2 to 16 μm, *Infrared Phys. Technol.* 52 (2009) 193–195.
- [4] K. Ankit, A. Varade, K. Reddy, D. Sarmistha, M. Chellamalai, Synthesis of high hardness IR optical coating using diamond-like carbon by PECVD at room temperature, *Diam. Relat. Mater.* 78 (2017) 39–43.
- [5] K.N. Reddy, A. Varade, A. Krishna, J. Joshua, D. Sasen, M. Chellamalai, P.V. Shashikumar, Double side coating of DLC on silicon by RF-PECVD for AR application, *Procedia Eng.* 97 (2014) 1416–1421.
- [6] O.M. Kutsay, A.G. Gontar, N.V. Novikov, S.N. Dub, V.N. Tkach, B.A. Gorshtein, O.V. Mozkova, Diamond-like carbon films in multilayered interference coatings for IR optical elements, *Diam. Relat. Mater.* 10 (2001) 1846–1849.
- [7] J. Amirloo, S.S. Saini, M. Dagenais, Comprehensive study of antireflection coatings for mid-infrared lasers, *J. Vac. Sci. Technol. A* 34 (2016) 061505.
- [8] G. Zhang, L. Guo, Z. Liu, X. Xiu, X. Zheng, Studies on diamond-like carbon films for antireflection coatings of infrared optical materials, *J. Appl. Phys.* 76 (1994) 705–707.
- [9] A. Miller, D. Reece, M. Hudson, C. Brierley, J. Savage, Diamond coatings for IR window applications, *Diam. Relat. Mater.* 6 (1997) 386–389.
- [10] J. Heeg, M. Rosenberg, C. Schwarz, T. Barfels, M. Wienecke, Optimised plasma enhanced chemical vapour deposition (PECVD) process for double layer diamond-like carbon (DLC) deposition on germanium substrates, *Vacuum* 83 (2008) 712–714.
- [11] A. Varade, K.N. Reddy, M. Chellamalai, P.V. Shashikumar, Diamond-like carbon coating made by RF plasma enhanced chemical vapour deposition for protective antireflective coatings on germanium, *Procedia Mater. Sci.* 5 (2014) 1015–1019.
- [12] D. Batory, A. Jedrzejczak, W. Szymanski, P. Niedzielski, M. Fijalkowski, P. Louda, I. Kotela, M. Hromadka, J. Musil, Mechanical characterization of a-C:H:SiO_x coatings synthesized using radio-frequency plasma-assisted chemical vapor deposition method, *Thin Solid Films* 590 (2015) 299–305.
- [13] K.D. Koshigan, F. Mangolini, J.B. McClimon, B. Vacher, S. Bec, R.W. Carpick, J. Fontaine, Understanding the hydrogen and oxygen gas pressure dependence of the tribological properties of silicon oxide-doped hydrogenated amorphous carbon coatings, *Carbon* 93 (2015) 851–860.
- [14] A. Jedrzejczak, L. Kolodziejczyk, W. Szymanski, I. Piwonski, M. Cichowski, A. Kisieleska, M. Dudek, D. Batory, Friction and wear of a-C:H:SiO_x coatings in combination with AISI 316L and ZrO₂ counterbodies, *Tribol. Int.* 112 (2017) 155–162.
- [15] S. Jana, S. Das, D. De, U. Gangopadhyay, P. Ghosh, A. Mondal, Effect of annealing on structural and optical properties of diamond-like nanocomposite thin films, *Appl. Phys. A* 114 (2014) 965–972.
- [16] D. Neerinc, Diamond-like nanocomposite coatings (a-C:H/a-Si:O) for tribological applications, *Diam. Relat. Mater.* 7 (1998) 468–471.
- [17] A. Tamulevičienė, Š. Meškinis, V. Kopustinskas, S. Tamulevičius, Multilayer amorphous hydrogenated carbon (a-C:H) and SiO_x doped a-C: H films for optical applications, *Thin Solid Films* 519 (2011) 4004–4007.
- [18] N. Moolsradoo, S. Abe, S. Watanabe, Thermal stability and tribological performance of DLC-Si-O films, *Adv. Mater. Sci. Eng.* 2011 (2011) 483437.
- [19] A.S. Grenadyorov, A.A. Solovyev, K.V. Oskomov, S.V. Rabotkin, Y.I. Elgin, V.S. Sypchenko, N.M. Ivanova, Effect of substrate bias and substrate/plasma generator distance on properties of a-C:H:SiO_x films synthesized by PACVD, *Thin Solid Films* 669 (2019) 253–261.
- [20] C. Venkatraman, C. Brodbeck, R. Lei, Tribological properties of diamond-like nanocomposite coatings at high temperatures, *Surf. Coat. Tech.* 115 (1999) 215–221.
- [21] S.J. Park, K.-R. Lee, D.-H. Ko, Tribochemical reaction of hydrogenated diamond-like carbon films: a clue to understand the environmental dependence, *Tribol. Int.* 37 (2004) 913–921.
- [22] W.J. Yang, Y.H. Choa, T. Sekino, K.B. Shim, K. Niihara, K.H. Auh, Thermal stability evaluation of diamond-like nanocomposite coatings, *Thin Solid Films* 434 (2003) 49–54.
- [23] L.K. Randeniya, A. Bendavid, P.J. Martin, M.S. Amin, E.W. Preston, Molecular structure of SiO_x-incorporated diamond-like carbon films; evidence for phase segregation, *Diam. Relat. Mater.* 18 (2009) 1167–1173.
- [24] F.L. Freire, C.A. Achete, G. Mariotto, R. Canteri, Amorphous nitrogenated carbon films: Structural modifications induced by thermal annealing, *J. Vac. Sci. Technol. A* 12 (1994) 3048–3053.
- [25] R.O. Dillon, J.A. Woollam, V. Katkanant, Use of Raman scattering to investigate disorder and crystallite formation in as-deposited and annealed carbon films, *Phys. Rev. B* 29 (1984) 3482–3489.
- [26] U. Muller, R. Hauert, B. Oral, M. Tobler, Temperature stability of fluorinated amorphous hydrogenated carbon films, *Surf. Coat. Tech.* 76–77 (1995) 367–371.
- [27] U. Muller, R. Hauert, Structural stability of Si-O-a-C:H/Si-a-C: H layered systems, *Mat. Res. Soc. Symp. Proc.* 434 (1996) 113–118.
- [28] S.A. Barve, S.S. Chopade, R. Kar, N. Chand, M.N. Deo, A. Biswas, N.N. Patel, G.M. Rao, D.S. Patil, S. Sinha, SiO_x containing diamond like carbon coatings: Effect of substrate bias during deposition, *Diam. Relat. Mater.* 71 (2017) 63–72.
- [29] W.J. Yang, T. Sekino, K.B. Shim, K. Niihara, K.H. Auh, Microstructure and tribological properties of SiO_x/DLC films grown by PECVD, *Surf. Coat. Tech.* 194 (2005) 128–135.
- [30] J. Bi, M. Yang, J. Peng, R. Sheng, L. Li, M.L. Yick, Effect of Si/O doping on the thermal stability of non-bonded hydrogenated diamond-like carbon coatings, *Surf. Coat. Tech.* 374 (2019) 1006–1014.
- [31] A.A. Ogwu, T.I.T. Okpalugo, J.A.D. McLaughlin, The effect of PECVD plasma decomposition on the wettability and dielectric constant changes in silicon modified DLC films for potential MEMS and low stiction applications, *AIP Adv.* 2 (2012) 032128.